Clays and Clay Minerals, Vol. 56, No. 3, 322–337, 2008.

HYDROTHERMAL SYNTHESIS, BETWEEN 75 AND 150ºC, OF HIGH-CHARGE, FERRIC NONTRONITES

ALAIN DECARREAU[1,*], SABINE PETIT[1], FRANÇOIS MARTIN[2], FRANÇOIS FARGES[3], PHILIPPE VIEILLARD[1], AND EMMANUEL JOUSSEIN[4]

[1] Université de Poitiers, UMR 6532 HydrASA CNRS/INSU, 40 Av. Recteur Pineau, F86022 Poitiers cedex, France
[2] ERT 1074 CNRS Géomatériaux, LMTG-OMP-UPS-IRD-CNRS, 14 Avenue Edouard Belin, F31400 Toulouse, France
[3] USM 201 – UMR.CNRS 7160, Muséum National d'Histoire Naturelle, 61 rue Buffon, F75005 Paris, France
[4] Université de Limoges, UMR 6532 HydrASA CNRS/INSU, 123 Av. A. Thomas, F87060 Limoges cedex, France

Abstract—High-charge nontronites were synthesized at 75, 90, 100, 110, 125, and 150ºC from a silico-ferrous starting gel with $Si_2FeNa_2O_6.nH_2O$ composition. This gel was oxidized in contact with air and then hydrothermally treated, for a period of 4 weeks, under equilibrium water pressure. The synthesized nontronites were similar to each other, regardless of the synthesis temperature. Their structural formula, obtained from chemical analysis, X-ray diffraction (XRD), and Fourier transform infrared (FTIR), Mössbauer, and X-ray absorption fine structure spectroscopies is: $(Si_{3.25}Fe^{3+}_{0.75})Fe^{3+}_2O_{10}(OH)_2Na_{0.75}$. A strictly ferric end-member of the nontronite series was therefore synthesized for the first time. The uncommon chemistry of the synthesized nontronites, notably the high level of Fe-for-Si substitution, induced particular XRD, FTIR, and differential thermal analysis-thermogravimetric analysis data. The ethylene glycol expandability of the synthetic nontronites was linked to their crystallinity and depended on the nature of the interlayer cation, moving from smectite to vermiculite-like behavior. As the synthesis temperature increased, the crystallinity of the synthesized clays increased. The nontronite obtained at 150ºC had the 'best crystallinity', which cannot be improved by increasing synthesis time or temperature.

Key Words—Clay Synthesis, FTIR Spectroscopy, High-charge Nontronite, Mössbauer Spectroscopy, XAFS.

INTRODUCTION

Most common smectites are Al-rich, but can present large chemical variability. The extended Al-for-Fe^{3+} substitutions of smectites, and their induced properties, are classically described by evolution between tetrahedral-octahedral-tetrahedral (TOT) phyllosilicate end-members. The smectitic end-members are beidellite (Al) and nontronite (Fe^{3+}) while the zero-charge smectites are pyrophyllite and ferripyrophyllite. Natural ferripyrophyllites have been studied previously (Chukhrov *et al*., 1979; Coey *et al*., 1984), with, for some of them, structural formulae very close to the theoretical end member $Si_4Fe^{3+}_2O_{10}(OH)_2$ (Badaut *et al*., 1992). In contrast, all natural nontronites contain more or less Al^{3+} either in their tetrahedral and/or octahedral sheets (Eggleton, 1977; Goodman *et al*., 1976; Gates *et al*., 2002). Using different protocols, weakly crystallized strictly ferric smectites have been synthesized (Decarreau and Bonnin, 1986; Decarreau *et al*., 1987). But these hisingerite-like, synthesized ferric smectites had no tetrahedral charge, and are, therefore, not equivalent to the nontronite end-member. Mizutani *et al.* (1991) obtained ferric smectites by hydrothermal treatments, at 100–200ºC, of mixtures of silicic acid, $FeSO_4$, NaOH, and dithionite. From Mössbauer data the synthesized smectites contain ~3% Fe^{2+}, and half of the Fe^{3+} cations are suggested to occur in tetrahedral sites; this appears to be completely unrealistic.

Thus, syntheses of Fe-smectites were performed in order to obtain strictly ferric nontronites with layer charges occurring by means of Fe^{3+}-for-Si tetrahedral substitutions only, and to track the evolution of smectite properties, according to the synthesis temperatures.

EXPERIMENTAL

Clay synthesis

Fe-smectites can be synthesized in either oxidizing or reducing conditions (see the review on smectite synthesis by Kloprogge *et al.*, 1999). Numerous papers show that ferric smectites can be more easily synthesized under partially reducing conditions (Harder, 1976; Decarreau and Bonnin, 1986; Farmer *et al.*, 1991; Mizutani *et al.*, 1991). Nagase *et al.* (1999) synthesized ferric smectites at 100ºC and 200ºC from starting gels with an Si/Fe/Mg ratio equal to 4/1.7/0.3, within the narrow pH range 12–12.4. At lower pH, X-ray amorphous products appear, while at pH >13, aegirine (Na, Fe silicate) and hematite precipitated.

So, the ferric smectites were synthesized using the procedure described by Decarreau and Bonnin (1986) and adjusted to obtain a coprecipitate gel with

* E-mail address of corresponding author:
alain.decarreau@hydrasa.univ-poitiers.fr
DOI: 10.1346/CCMN.2008.0560303

$Si_2FeNa_2O_6$ composition. The gel was obtained by mixing solutions of sodium silicate and ferrous chloride.

After precipitation, the gel was recovered by filtration and washed using a few mL of deionized water to prevent gel dissolution and to remove NaCl, and then dehydrated at 60ºC for 48 h before grinding. About 5 g of gel were prepared. Initially dark blue, the gel became brown-yellow after dehydration, due to the oxidation of Fe. 500 mg of powdered gel and 30 mL of deionized water were then placed in Teflon-coated metallic bombs. The starting pH was adjusted to 12.5 by adding drops of 1 M NaOH. Syntheses were performed, over a 4-week period, under equilibrium vapor pressure at 75, 90, 100, 125, and 150ºC (±2ºC), higher temperatures promoting the crystallization of aegirine (Decarreau *et al.*, 2004). At the end of the synthesis, the solid phases were separated by filtration and dried overnight at 40ºC.

Analyses

The pH before (pHi) and after (pHf) synthesis was measured at 25ºC on the quenched liquid phases. The Na, Si, and Fe aqueous concentrations were measured by atomic absorption spectrometry (AAS) (Perkin Elmer 3110 apparatus). The chemistry of solids was determined from powder-pressed disks (5 mm in diameter, 1 mm thick), using a Scanning Electron Microscope (SEM) (JEOL JSM 5600L apparatus) equipped with an EDX energy dispersive spectrometer. Chemical analyses were performed at 15 kV operating voltage and 2.5 nA operating current, in order to prevent any damage to the clay minerals or element migration during analysis. Analyses were calibrated using reference clay samples. Under these conditions the analytical error for each element is 1%.

The XRD patterns were recorded using a Philips PW 1730 diffractometer (Fe-filtered CoKα radiation generated at 40 kV and 40 mA, proportional detector, 0.1 divergence slit, 1º receiving slit, scans taken over 3–80º2θ, step interval 0.02º, counting time 6 s) equipped with a stepping motor drive in the goniometer (SOCABIM DACO system). The XRD patterns were obtained from powders and oriented preparations of Na- and Ca-saturated samples in the air-dried (AD) state, after ethylene glycol (EG) solvation, and after heating (250ºC, 4 h).

The layer charge of the synthesized clays was estimated by XRD after saturation of samples with C_{12}-alkylammonium (Olis *et al.*, 1990). The preparation of the alkylammonium derivatives follows the recommendations of Lagaly (1994). The layer charge was determined following the procedure of Gillot *et al.* (2001).

The XRD patterns of Ca-saturated samples, after EG solvation, were simulated using the *Newmod*® program (Reynolds, 1985). Simulations were carried out for mixed-layer materials with various proportions of one-layer and two-layer EG complexes, and with *N* (number of layers in the stacking sequence) in the range 5–10.

Fourier transform infrared (FTIR) spectra were recorded at 4 cm^{-1} resolution in transmission mode in the 4000–400 cm^{-1} range with a Nicolet 510 FTIR spectrometer which was continuously purged with dry air containing substantially less CO_2 than normal air. Spectra were obtained from KBr pressed pellets dried overnight at 110ºC to suppress adsorbed water. These pellets, 2 cm in diameter, were prepared by mixing 3 or 4 mg of sample with 300 mg of KBr in order to obtain well defined spectra with optical density or absorbance of <2. Spectral manipulations were performed using the OMNIC software package (Nicolet Instruments Corp.). Band component analysis was carried out using the least-squares fitting program *Peak Solve* with the Gauss-Lorentz form of each component. The goodness of the fit is given by the linearity of the residual component.

^{57}Fe Mössbauer absorption spectra over the range ±4 mm/s in 512 channels were recorded at the Laboratoire de Chimie de Coordination (Toulouse, France). The Mössbauer spectrometer consists of a compact detector γ-system for high counting rates and a Wissel conventional constant-acceleration Mössbauer velocity transducer. A ^{57}Co (in Rh) source with nominal activity of 50 mCi was used. The spectra were obtained at room temperature, specifically at 80 K, and recorded on a multichannel Canberra analyzer attached to a computer. The isomer shift was recorded with respect to α-Fe metal. According to Rancourt *et al.* (1993), the absorber sample thickness was approximated at ~100 mg of mineral cm^{-2} for nontronites. Powders were finely ground under acetone and placed in the Plexiglas sample holder. Lorentzian line shapes were assumed for deconvolutions, based on least-squares fitting procedures. χ^2 was used to measure the quality of the computer fit.

For the Na-exchanged clay synthesized at 150ºC, fluorescence-yield Fe K-edge X-ray absorption near-edge spectroscopy (XANES) spectra were collected on beamline 11-2 at the Stanford Synchrotron Radiation Laboratory (SPEAR3 storage ring, Stanford, USA). The spectra were collected under high-resolution conditions (Si (220)), using a double-crystal monochromator and 0.3 mm high vertical aperture slits before and after the monochromator (details in Farges, 2004). A 3 µm hematite foil was used to check the energy reproducibility at the 0.05 eV energy level. The fluorescence spectra were collected using a Stern-Heald detector with a 3 µm Mn filter (to filter the elastic scattering) with the sample positioned at 90º to minimize self-absorption effects (which were observed to be negligible). Two other samples were analyzed: a natural (unheated) nontronite from Garfield (from the Stanford mineral collection), and a heated counterpart (500ºC in air for 3 h). Finally, $FePO_4$ served as a model for Fe(III) in a T_d geometry. Pre-edge features were analyzed by modeling simultaneously the pre-edge and the background with a

continuum of pseudo-Voigt shaped peaks fixed by core-hole lifetime (~1.0 eV; (Farges *et al.*, 2004)) and experimental resolution (here, 0.7 eV). In contrast to Gates *et al.* (2002), arctangent-based baselines were avoided in the present study because they overestimate the actual intensities/areas by as much as 20%. This is because of the presence of additional transitions at a few eV above the pre-edge feature that convolutes the originally shaped arctangent atomic step function (Farges *et al.*, 2004). Background-corrected pre-edge spectra for the two 'high-temperature' nontronites ('synthetic clay' and 'heated Garfield') were then modeled by linear combination of the pre-edge features for the unheated Garfield nontronite and $FePO_4$.

Thermal analyses were carried out on ~20 mg of samples with a NETZSCH Simultan STA 409 EP analyzer. Differential thermal analysis-thermal gravimetric (DTA-TG) data were collected in air using a 10ºC/min heating rate over the 20−1100ºC temperature range.

RESULTS

Chemical analyses

At the end of the synthesis, the solutions were clear, with no yellow discoloration due to Fe dissolution (Fe concentrations were always found to be below the detection limit: 0.5 mg L^{-1}). During syntheses, the pH was either constant or increased slightly (Table 1). A pH >12 induced dissolution of silica. From Si concentrations in solution (Table 1), and taking into account the loss of water vapor during synthesis, by mass balance calculation, ~15% of the starting gel silica was dissolved. Some of the Na in solution arises from addition of NaOH, but 70−80% comes from gel dissolution.

The end-of-synthesis, solid sample obtained at 150ºC was analyzed after Ca saturation. Only Si, Fe, and Ca were detected. Sixteen localized analyses (~1 μm^2) were made, with the results all being very similar (Table 2). The data show that the end-of-synthesis solid contains less silica than the starting gel. Chemical data obtained on the liquid and solid phases are consistent: all Fe is in the synthetic clay, while some silica and most of the Na is in solution at the end of synthesis.

Table 1. Chemical properties of end-of-synthesis solutions.

T (ºC)	75	90	100	110	125	150
pHf	12.56	12.53	12.54	12.68	12.60	12.52
Si (g L^{-1})	0.54	n.a.	0.80	n.a.	n.a.	0.84
Na (g L^{-1})	2.32	n.a.	2.58	n.a.	n.a.	2.15

T: synthesis temperature
n.a.: not analyzed

XRD data

The powder XRD pattern of the starting gel (Figure 1) shows two very broad bands at 3.05 and 1.55 Å, and a broad basal reflection at 13.6 Å. This latter feature can be interpreted as a broad 001 reflection of a TOT-like structure having two layers of water in the interlayer. The starting gel is very poorly organized, but contains some TOT-like layered structures.

The powder XRD pattern of the solid phase, obtained at 150ºC, shows a narrow 001 reflection at 11.96 Å and dissymmetric (*hk*) bands at 4.57 Å ($02\bar{1}\bar{1}$), 2.56 Å ($13\bar{2}\bar{0}$), 1.72 Å ($15\bar{2}\bar{4}\bar{3}\bar{1}$) and 1.54 Å ($06\bar{3}\bar{3}$) (Figure 1). The reasonably symmetric band at 3.09 Å is probably the 004 reflection. There is no diffracted intensity at low angles, before the 001 peak, indicating a lack of interstratification. At higher angles, diffracted intensities reach the base line suggesting the lack of amorphous product. This sample therefore contains a pure Na-saturated smectite. A d_{001} distance of 12 Å is due to a single water layer, in accordance with a sodic smectite (Brindley and Brown, 1980). The mean crystal coherency was measured (using the Scherrer equation) from the width of the 001 and 06-33 reflections; along the *c** direction the coherency was 95 Å (about eight staked layers) and 120 Å in the (*a*,*b*) plane.

When the synthesis temperature decreases (Figure 1), the *hk* and 00*l* reflections are broadened, but stay at the same position. At low angles, before the 001 maximum, diffracted intensities increase with the decrease of synthesis temperatures. All these features are consistent with a decrease in the crystallinity of the synthetic smectite clay when the synthesis temperature decreases from 150 to 75ºC.

After heating, 001 reflections near 10 Å were observed, indicating a collapse of all the layers.

Table 2. SEM-EDX chemical analyses of the Ca-saturated synthetic clay obtained at 150ºC.

	Si	Ca	Fe
	3.21	0.38	2.75
	3.2	0.41	2.77
	3.28	0.39	2.67
	3.19	0.37	2.79
	3.16	0.37	2.83
	3.18	0.4	2.78
	3.2	0.37	2.79
	3.21	0.4	2.75
	3.22	0.39	2.73
	3.23	0.4	2.71
	3.32	0.37	2.61
	3.22	0.39	2.74
	3.21	0.4	2.72
	3.11	0.4	2.89
	3.26	0.4	2.67
Mean	3.21	0.39	2.75

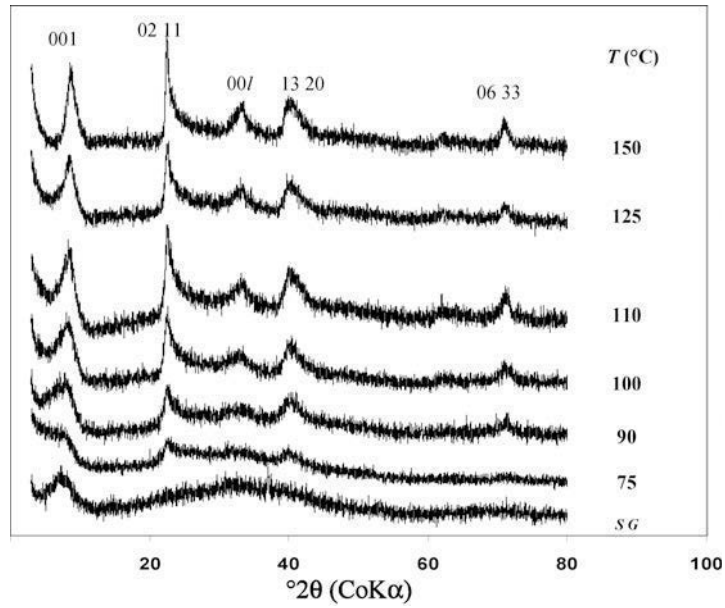

Figure 1. Powder XRD patterns of synthesized nontronites. *T* is the synthesis temperature. *SG* is the staring gel.

After ethylene-glycol treatment, the XRD patterns differ according to the interlayer cation. For Na-saturated samples (Figure 2), d_{001} distances at 12.54 Å were observed for smectites synthesized at 150 and 125ºC (one-layer EG complex), 16.54 Å (two-layer EG complex) for the 100ºC sample and intermediate values, and 14.86 Å and 15.3 Å for the 110ºC and 90ºC samples, respectively, corresponding to mixed-layer, EG complexes. For the 75ºC sample, the 001 reflection is very broad (some stacked layers only) with maximum intensity at 15.3 Å. For Ca-saturated samples (Figure 3), the d_{001} values were between 15.5 Å (150ºC sample) and 16.1 Å (90 and 100ºC samples), with intermediate values for other samples (15.9 Å, 75ºC sample; 15.7 Å, 110ºC sample; 15.8 Å, 125ºC sample). Using the *Newmod*® program, these distances correspond to random mixed layers of one-layer EG and two-layer EG complexes (55–70% of two-layer EG complexes). As previously for hydrated samples, the 001 reflections for EG-saturated samples broaden when the synthesis temperature of samples decreases.

After C_{12}-alkylammonium saturation, the XRD pattern of the sample synthesized at 150ºC shows a narrow, strong symmetric peak at 23.6 Å (Figure 4). According to Olis *et al.* (1990), this reflection indicates a paraffin-type configuration and then a layer charge $\geqslant 0.75$ per $O_{10}(OH)_2$.When the synthesis temperature decreases, the peak maxima stay at the same position but become broadened. From these data we can conclude that, whatever the temperature at which the smectites were synthesized, their layer charge is always $\geqslant 0.75$ per $O_{10}(OH)_2$, the broadening of the peak being linked, as above, to a decrease in the crystallinity of the clays.

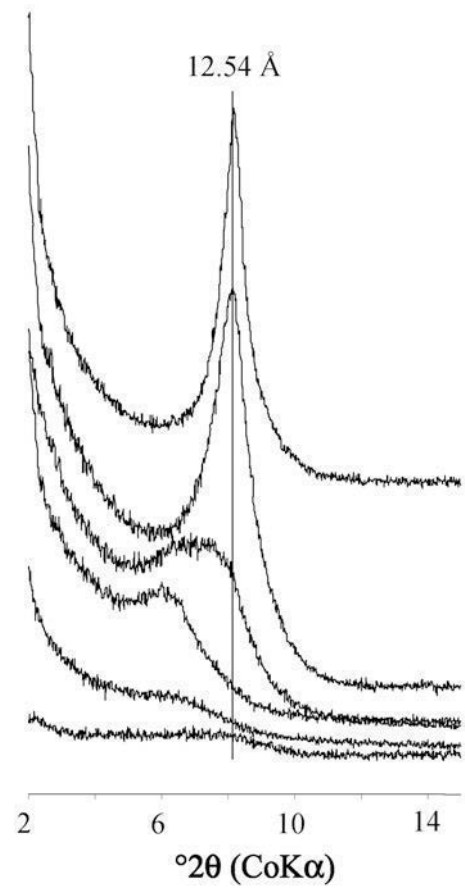

Figure 2. XRD patterns of glycolated Na-saturated nontronites synthesized (from lowest to uppermost trace) at 75, 90, 100, 110, 125, and 150ºC.

TEM data

Particles of synthesized smectites are crumpled flakes with rolled edges, associated in micron-sized aggregates (Figure 5). When the synthesis temperature increases, particles are darker and then thicker, with no significant change in particle or aggregate size. Electron diffraction patterns of the thinnest particles exhibit rings of several hexagonal dots.

DTA-TG data

The DTA-TG curves of all the Na-saturated samples exhibited two endothermic events, one just below 100ºC and a second in the range 373−393ºC (Table 3). The first event corresponds to the loss of adsorbed water. The second event can undoubtedly be attributed to the dehydroxylation of the smectite. Mackenzie (1970) showed that chemical composition and structural order affect the dehydroxylation temperature of TOT clays. The occurrence of Fe in clay structures tends to reduce the dehydroxylation temperature, either for kaolinites (Iriarte *et al.* 2005) or for smectites (Brigatti, 1983). For nontronites, Brigatti (1983) observed a good negative correlation between the dehydroxylation temperature and the Fe content. For the reference 'Garfield' nontronite, Bonnin (1981) measured a dehydroxylation temperature of 458ºC. The dehydroxylation temperatures measured here are <400ºC, and would be correlated with the high Fe contents of these strictly ferric nontronite-like clays.

Drits *et al.* (1995) and Muller *et al.* (2000) show that dioctahedral TOT clays with *trans*-vacant (*tv*) octahedra are characterized by dehydroxylation temperatures 150−200ºC lower than those of the same clays with *cis*-vacant octahedra (*cv*). Reference nontronites, notably the 'Garfield', are well known to have a *tv* structure (Besson *et al.*, 1983; Tsipursky and Drits, 1984). The dehydroxylation temperatures measured for the synthetic clays are therefore consistent with a *tv* structure.

The dehydroxylation temperature decreases from 393 to 373ºC when the synthesis temperature decreases from 150 to 75ºC.

The mass loss of samples around the second endothermic peak was used to estimate the quantity of smectite formed during synthesis (Table 3) (on the basis of a theoretical mass loss of 3.92% for a ferric smectite having the mean chemical composition given in Table 2). For syntheses performed at 125ºC and 150ºC, almost all of the starting gel is transformed into smectite, and the amount of smectite formed is reduced by up to 60% for the lower temperature.

Mössbauer data

Decomposition of Mössbauer spectra, obtained at 80 and 293 K, into three quadrupole doublets (Figure 6) gave a good fit (χ^2 = 1.99 at 80 K, and 1.479 at 293 K). Addition of further doublets did not improve significantly the goodness of the fit. Mössbauer parameters of the doublets are very similar for the spectra obtained at different temperatures (Table 4), showing the consis-

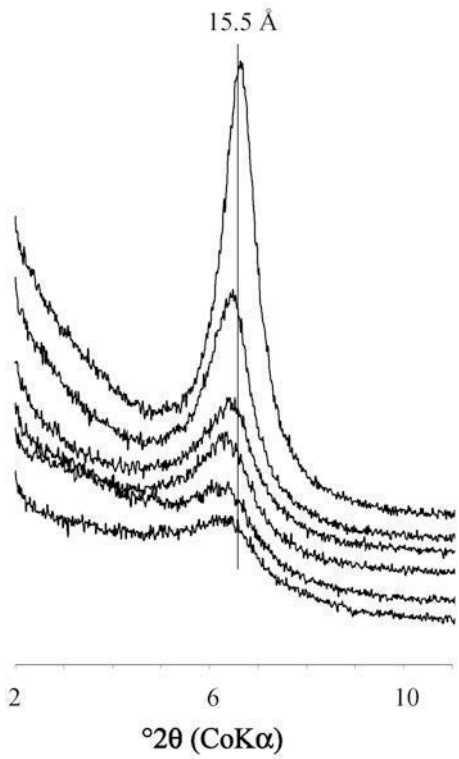

Figure 3. XRD patterns of glycolated Ca-saturated nontronites synthesized (from lowest to uppermost trace) at 75, 90, 100, 110, 125, and 150ºC.

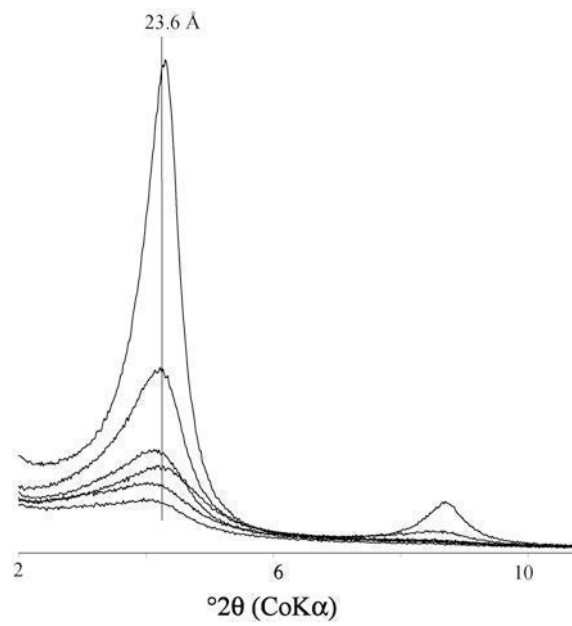

Figure 4. XRD patterns of C_{12}-alkylammonium-saturated nontronites synthesized (from lowest to uppermost trace) at 75, 90, 100, 110, 125, and 150ºC.

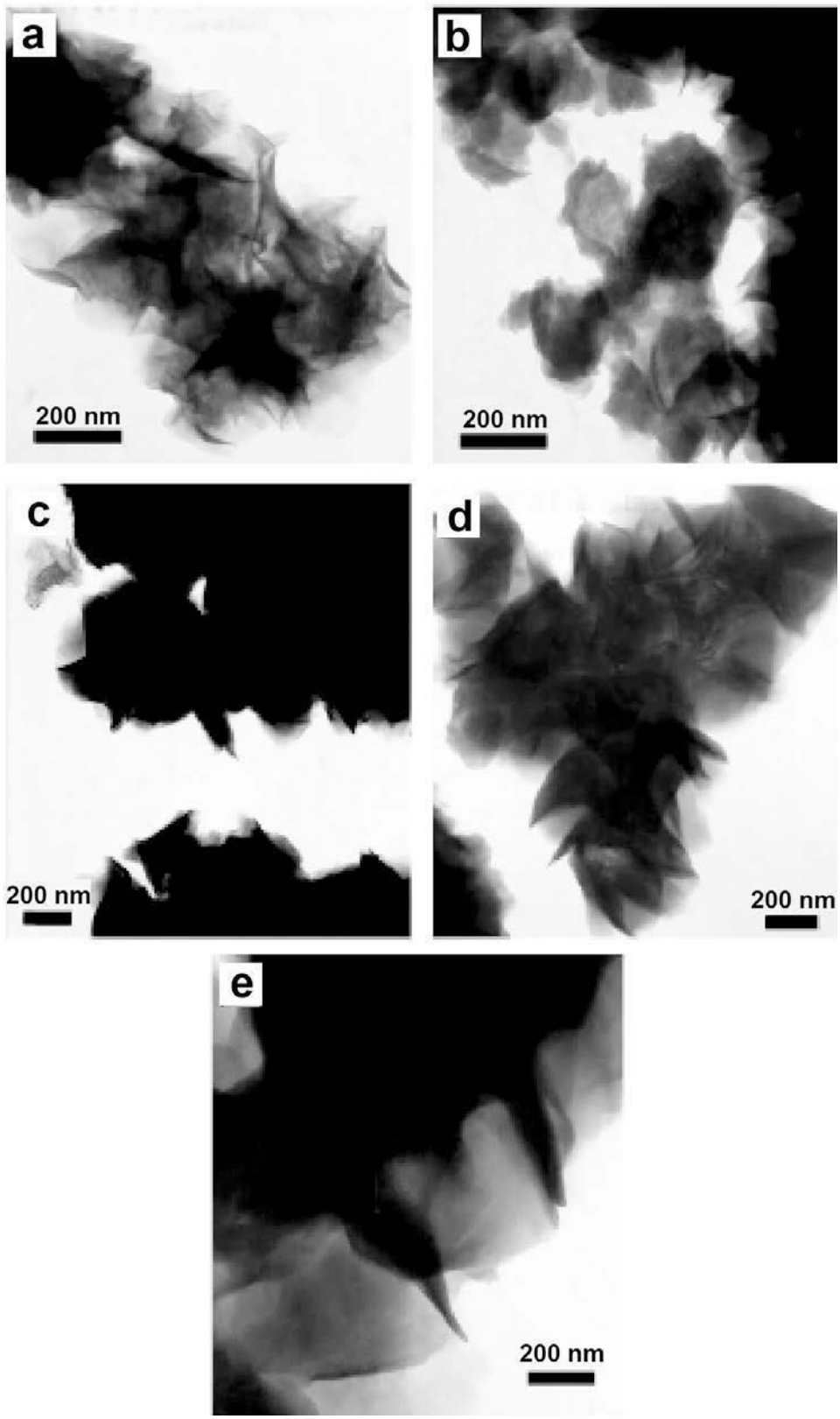

Figure 5. TEM images of nontronites synthesized at (a) 75, (b) 90, (c) 110, (d) 125, and (e) 150ºC.

Table 3. DTA-TG data of the Na-saturated synthesized clays.

T (ºC)	Endo.1 (ºC)	Endo.2 (ºC)	Weight loss (%) (Endo. 2) ±0.2	TOT clay (%) (1)
150	95	393	−3.4	87
125	99	382	−3.72	95
110	98	377	−3.0	76
100	98	377	−2.35	60
90	98	375	−2.5	65
75	98	375	−2.25	60

T: synthesis temperatures
Endo.1 (ºC), Endo.2 (ºC): temperatures of first and second endothermic events.
(1): The % of synthesized TOT clay was estimated using the weight loss measured by TG during the second endothermic event (280−500ºC), and assuming 3.92 wt.% OH in the structural formula of the synthetic clays (Table 2).

tency of the decomposition (Coey, 1984). Isomer shifts (IS) and quadrupole splitting (QS) values (Table 4) are typically those of Fe^{3+} ions (Coey, 1980), confirming the complete oxidation of Fe during the synthesis. As classically observed for Fe^{3+} Mössbauer parameters, at low temperature, line widths are narrower, IS values are larger, and QS values are clearly not temperature dependent (Coey, 1984).

The small IS values of doublet 1 (Table 4) are typically those of tetrahedrally coordinated Fe^{3+} in nontronites (Goodman *et al.*, 1976; Goodman, 1978; Besson *et al.*, 1983; Luca, 1991). Mössbauer parameters of the other two doublets are those of octahedrally coordinated Fe^{3+} in phyllosilicates.

Doublet 2 (Table 4) is characterized by small QS values, which were observed previously in Mössbauer spectra of ferripyrophyllite, and were attributed to Fe^{3+} in *M*2 (*cis* hydroxyls) quite regular octahedral sites surrounded by three other octahedral Fe^{3+} (Coey *et al.*, 1984; Badaut *et al.*, 1992). The QS values observed for the synthesized TOT clays are larger (0.271 mm s^{-1} at 293 K) than those observed for ferripyrophyllite (0.18−0.20 mm s^{-1}), suggesting slightly more distorted octahedra.

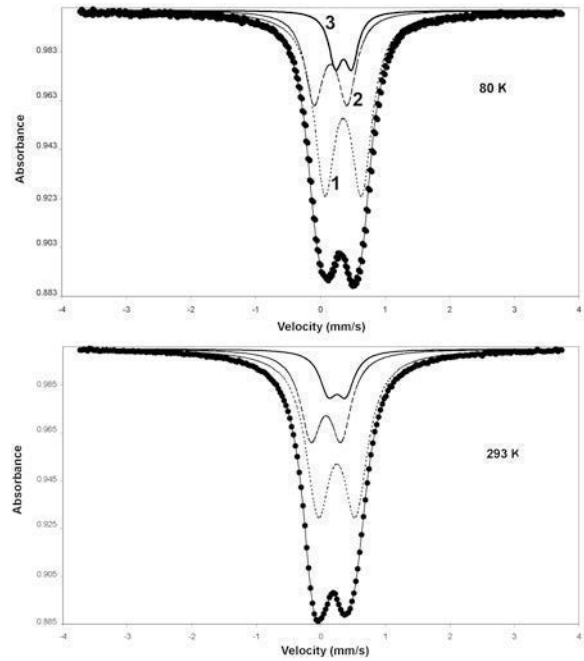

Figure 6. Mössbauer spectra (80 and 293 K) of nontronite synthesized at 150ºC. Dots = experimental spectra. Parameters of doublets 1, 2, and 3 are given in Table 4.

The QS values near or above 0.6 mm s^{-1}, as observed for doublet 3, have often been attributed to Fe^{3+} in *M*1 (*trans* hydroxyls) octahedra (Goodman *et al.*, 1976; Heller-Kallai and Rozenson, 1981). Taking into account the relative intensity of this doublet (Table 4) and the chemistry of synthesized TOT clay (Table 2), it represents ~1.6 Fe atoms per formula unit (a.p.f.u.). In accordance with DTA data, this doublet cannot be attributed to *M*1 sites.

Another possible approach is to calculate the values of Mössbauer parameters, using Electric Field Gradient (EFG) calculations, based on the point charge model of Goodman (1976), or on molecular orbital calculations by Mineeva (1978). Goodman (1978) first suggested that the two doublets observed in Mössbauer spectra of nontronites might be explained by the possible occurrence of Al

Table 4. Computer fitting parameters of Mössbauer spectra shown in Figure 6.

	Doublet 1		Doublet 2		Doublet 3	
	80 K	293 K	80 K	293 K	80 K	293 K
IS (mm s^{-1})	0.28	0.203	0.48	0.37	0.48	0.374
QS (mm s^{-1})	0.509	0.466	0.25	0.271	0.566	0.577
LW (mm s^{-1})	0.343	0.385	0.244	0.324	0.39	0.459
RI (%)	28	28	11	11	61	61

IS: isomer shift
QS: quadrupole splitting
LW: line width
RI: relative intensity

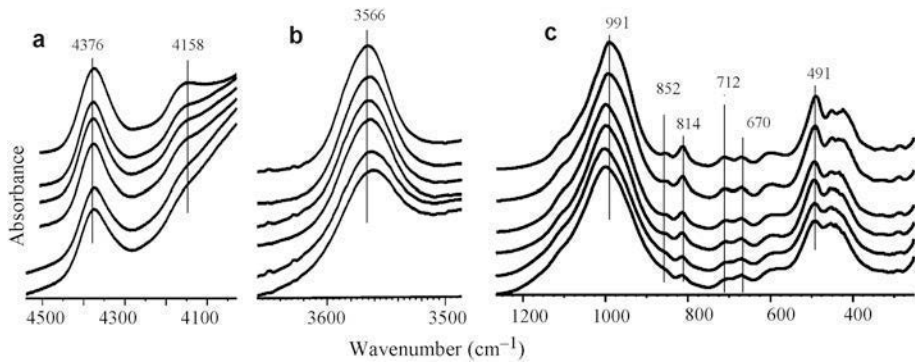

Figure 7. FTIR spectra of nontronites synthesized (from lowest to uppermost trace) at 75, 90, 100, 110, 125, and 150ºC. (a) OH combination region; (b) OH-stretching region; (c) 1200−300 cm^{-1} region.

and/or Fe^{3+}-for-Si substitutions. This interpretation was then proved by EFG calculations carried out by Besson *et al.* (1983) and by Daynyak and Drits (1987). These models allow us to take into account the cationic environments of Fe^{3+} both in octahedral and in tetrahedral sheets. For smectite with a *tv* structure such as nontronite, the doublet with a low QS value (0.28−0.35 mm s^{-1}) (doublet 2, Table 4) is thus attributed to Fe^{3+} in *M*2 sites surrounded by [4Si](3R^{3+}), while the doublet with QS values within the range 0.6−0.8 mm s^{-1} (doublet 3, Table 4) may be attributed to Fe^{3+} in *M*2 sites surrounded by [3SiR^{3+}](3R^{3+}).These attributions of doublets 2 and 3 are consistent with the large amounts of tetrahedral Fe in the synthesized smectite.

MIR and NIR data

MIR OH-stretching region. As for natural nontronites (Goodman *et al.*, 1976; Gates, 2005), MIR spectra in this region show an absorption band near 3560−3566 cm^{-1} for all samples, due to Fe_2^{3+}-OH stretching modes (Figure 7). From decomposition, this band can be modeled using one component only (Figure 8). The position of the band moves slightly to higher values when the synthesis temperature increases (Table 5) while, simultaneously, the bandwidth decreases. The evolution of IR parameters is clearly linked to the increase in the nontronite crystallinity with synthesis temperature. Natural nontronites are probably similar to the synthesized nontronite obtained at 150ºC. As the synthesized nontronites contain only Fe^{3+} cations, the IR parameters given in Table 5 are those of Fe_2^{3+}-OH-stretching bands in nontronites. By comparison with previous spectral decomposition of IR spectra of Fe-rich dioctahedral TOT clays (glauconites, celadonites, smectites) (Slominskaya *et al.* 1986; Madejová *et al.*, 1994; Besson and Drits, 1997), it appears that: one band only is sufficient for the model of the Fe_2^{3+}-OH-stretching mode; the wavenumber of νFe_2^{3+}-OH in nontronites (3566 cm^{-1}) is significantly larger than those for Fe-rich micas such as glauconites and celadonites (3530−3545 cm^{-1}) as already stated by Zviagina *et al.* (2004).

MIR SiO band. The position of the strong Si−O stretching band moves slightly from 1004 to 991 cm^{-1} when the synthesis temperature increases (Figure 7). The exact position of this band is known to shift to lower frequencies when the octahedral Fe^{3+} content (Gates, 2005), and especially the tetrahedral Fe^{3+} content (Goodman *et al.*, 1976), increases. The smallest wavenumber observed by Goodman *et al.* (1976) was 1001 cm^{-1}, for a nontronite having the following composition (per$O_{20}(OH)_4$): $(Si_{6.21}Al_{0.14}Fe_{1.65})(Fe_{4.04}Mg_{0.21})$. A wavenumber of 991 cm^{-1} for the Si−O stretching band is, as far as the authors are aware, the lowest observed in IR spectra of nontronites. Synthesized nontronites differ from the sample studied by Goodman *et al.* (1976) by a higher tetrahedral charge due only to Fe substitution and the lack of octahedral Mg. According to Goodman *et al.* (1976), octahedral Mg has a smaller effect on the Si−O band wavenumber than the level of tetrahedral Fe-for-Si substitution. The 991 cm^{-1} frequency observed here for the Si−O band, is mostly due to the large amount of tetrahedral Fe^{3+}. For synthesized nontronites, which always have the same chemistry and the same layer charge, the shift of the Si−O band from 1004 to 991 cm^{-1} when the synthesis temperature increases is probably related to the crystallinity of the clays and/or to the amount of unreacted starting gel.

MIR OH-bending region. Two bands at 852 and 814 cm^{-1} appear, the former being more resolved when the synthesis temperature (and therefore the

Table 5. Frequency and line width (LW) obtained after decomposition of MIR and NIR spectra. (All data in cm^{-1}.)

T (ºC)	νFe_2^{3+}-OH	LW	$(\nu + \delta)Fe_2^{3+}$-OH	L.W.
75	3565	59	4374	79
90	3565	55	4374	77
100	3566	51	4376	73
110	3566	49	4377	73
125	3566	47	4377	74
150	3568	45	4375	76

T: synthesis temperature

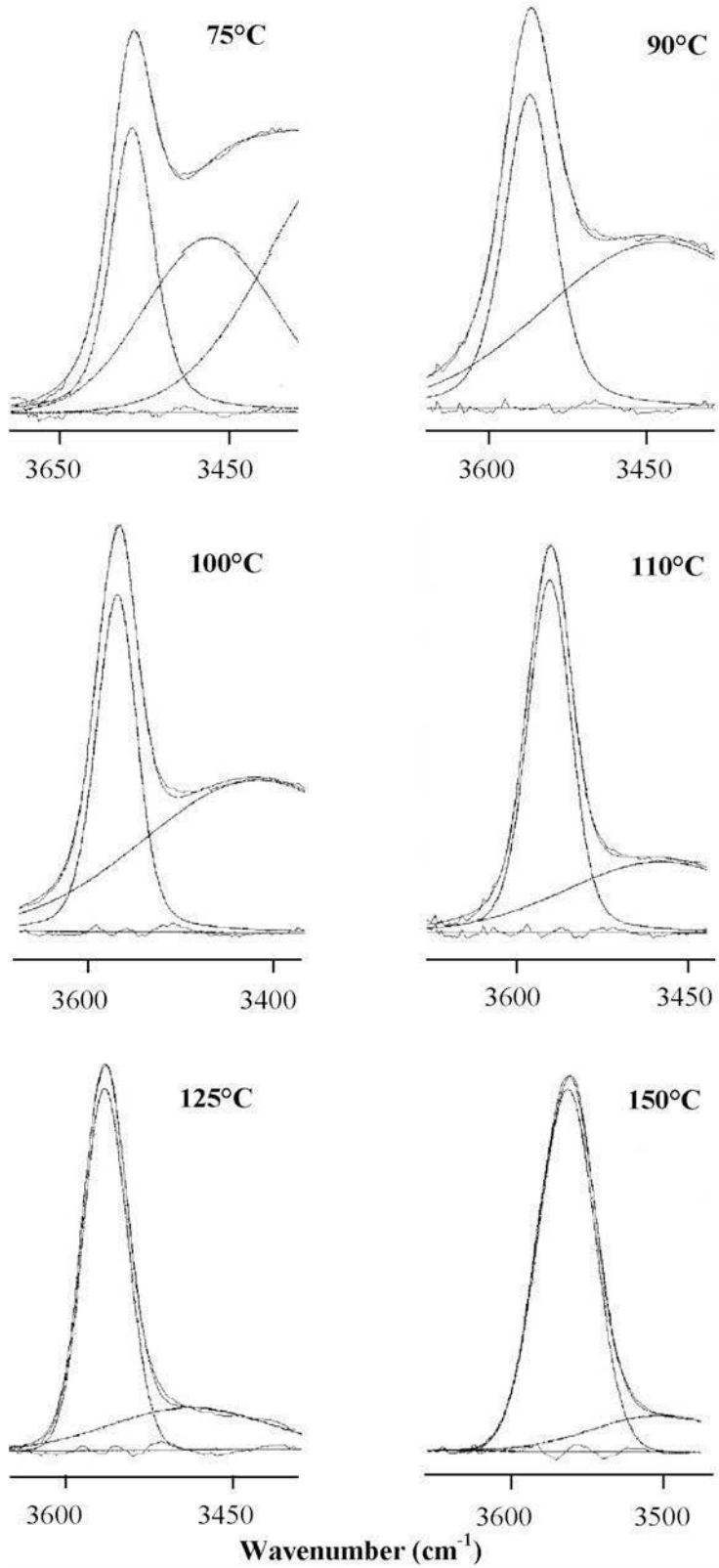

Figure 8. Decomposition of FTIR spectra in the OH-stretching region of synthesized nontronites. Elementary components are plotted and the residual lines show the difference between the fit and the experimental curve. Broad bands at lower frequencies are due to water.

crystallinity) of the nontronites increases (Figure 7). The 814 cm^{-1} band is well known and clearly attributed to the Fe_2^{3+}-OH-bending mode (Gates, 2005). For nontronites with >2.5 Fe^{3+} per $O_{10}(OH)_2$, Gates (2005) and Keeling *et al.* (2000) assigned a band near 850 cm^{-1} to a second Fe_2^{3+}-OH bending mode. During reduction experiments of Garfield nontronite, Fialips *et al.* (2002) observed a rapid loss of the 844 cm^{-1} equivalent band, showing clearly its link with the occurrence of octahedral Fe^{3+}. This band was not observed in IR spectra of poorly crystallized, hisingerite-like, synthetic Fe-smectites with little or no Fe-for-Si tetrahedral substitution (Decarreau and Bonnin, 1986; Decarreau *et al.*, 1987). Therefore, the occurrence of a band near 850 cm^{-1} in natural and synthetic nontronites is probably related to a high level of octahedral Fe^{3+} in relatively well crystallized nontronites. Both the MIR Fe_2^{+}-OH stretching band and the NIR Fe_2^{3+}-OH combination band (stretching + bending, 4376 cm^{-1}) (see below) of synthetic nontronites could be decomposed satisfactorily using just a single component. The assignment of the 852 cm^{-1} band to a second Fe_2^{3+}-OH-bending mode proposed by Gates (2005) and Keeling *et al.* (2000) is still open for discussion.

MIR 700-400 cm^{-1} region. Bands near 424, 451, 491, 589, and 670 cm^{-1} are classically observed in IR spectra of nontronites (Goodman *et al.*, 1976). As their frequencies are clearly affected by the amount of octahedral Fe^{3+}, they are interpreted as lattice bands including $Fe^{3+}{}_{oct}$–O bonds (Gates, 2005). A new band at 712 cm^{-1} (Figure 7) is observed in IR spectra of the synthesized smectites studied here. Such a band is absent in IR spectra of natural nontronites (Goodman *et al.*, 1976; Gates, 2005) and of ferric smectites without Fe-for-Si tetrahedral substitution (Decarreau and Bonnin, 1986; Decarreau *et al.*, 1987). This seems to be related to the high level of Fe-for-Si tetrahedral substitution of these synthetic nontronites and is probably due to tetrahedral Fe^{3+}–O vibrations.

NIR spectra. Clear bands appear at 6984 cm^{-1} (not shown), 4376 cm^{-1}, and a shoulder at 4158 cm^{-1} (Figure 7). The 6984 cm^{-1} band is the overtone of the 3566 cm^{-1} stretching band. The combination band OH-stretching and bending modes at 4376 cm^{-1} was decomposed using a single component, whatever the synthesis temperature, and gave a reasonably constant band position with few variations in bandwidth (Table 5). The shoulder at 4158 cm^{-1} increases with synthesis temperature (Figure 7) and is not attributed unambiguously.

X-ray absorption fine structure (XAFS) spectroscopy. The pre-edge spectra (Fe K-edge) of the nontronite obtained at 150ºC and of the Garfield nontronite are shown in Figure 9. After Manceau *et al.* (2000) and Gates *et al.* (2002), the Garfield nontronite is taken as a reference nontronite containing only octahedral Fe^{3+}. Its pre-edge spectrum is characterized by low intensity due to the forbidden 1s → 3d transition for Fe^{3+} in an ideal octahedral environment (Calas and Petiau, 1983). The split of the Garfield pre-edge is due to 1s → 3d t_2 and e_g transitions (labeled A1 and A2; Figure 9b), observed when Fe^{3+} ions are located in a regular octahedron (Manceau *et al.*, 2000). Using core-hole lifetime width (1 eV) and experimental widths (0.7 eV), no other transition is needed to model the pre-edge, in agreement with Westre *et al.* (1997). The simultaneous decomposition of the pre-edge and its baseline show that A1 and A2 have similar intensities (Figure 9c). The Fe K-edge spectra for heated nontronite (500ºC; Figure 9d) also exhibit a doublet but with a much greater intensity than unheated nontronite. However, this pre-edge requires three transitions (A1, A2, and A3) to be modeled with the energy-width constraints above. Such pre-edge decomposition is consistent with the presence of a highly distorted octahedron around Fe^{3+}, as in epidote (Wilke *et al.* 2001). Therefore, no evidence of C3v (trigonal bipyramid; Farges *et al.*, 2004) geometry is found around Fe^{3+} in heat-treated nontronite, as A3 should be much lower in intensity (Westre *et al.*, 1997). However, A2 can also arise from T_d moieties (mixed with O_h in the ratio ~10:90). Based on pre-edge analysis alone, one cannot differentiate between the two models (highly distorted O_h or a mixture of O_h and T_d). In contrast, the spectrum of the synthesized nontronite is symmetrical with a high intensity (Figure 9e). The constrained model of the pre-edge and its baseline resulted in a triplet with A2 that is much greater than A1 and A3 (Figure 9d). Only the presence of both T_d and O_h geometries can explain such a decomposition.

These features are typical of dioctahedral smectites with a high level of tetrahedral Fe^{3+} and/or Fe^{3+} ions in distorted octahedra, notably when the octahedral sheet contains appreciable amounts of Al or Mg (Manceau *et al.*, 2000; Gates *et al.*, 2002). The pre-edge spectrum of the synthesized nontronite is about three times more intense when compared to the pre-edge spectrum of the reference NG-1, Hohen Hagen, Germany, nontronite (>10% of the Fe^{3+} in tetrahedral sites, Gates *et al.*, 2002), indicating a high level of Fe in the tetrahedral sheet. The experimental pre-edge spectrum of the synthesized nontronite was then simulated by mixing spectra of Garfield nontronite (octahedral Fe^{3+}) and $FePO_4$ (tetrahedral Fe^{3+}). The best fit was obtained for 30% tetrahedral Fe^{3+}.

DISCUSSION

Synthesized clays

We know from the XRD information that the synthesized clays are Fe-smectites. C_{12}-alkylammonium saturation results indicate a layer charge of $\geqslant 0.75$ per $O_{10}(OH)_2$. Mössbauer and XAFS spectroscopy confirm

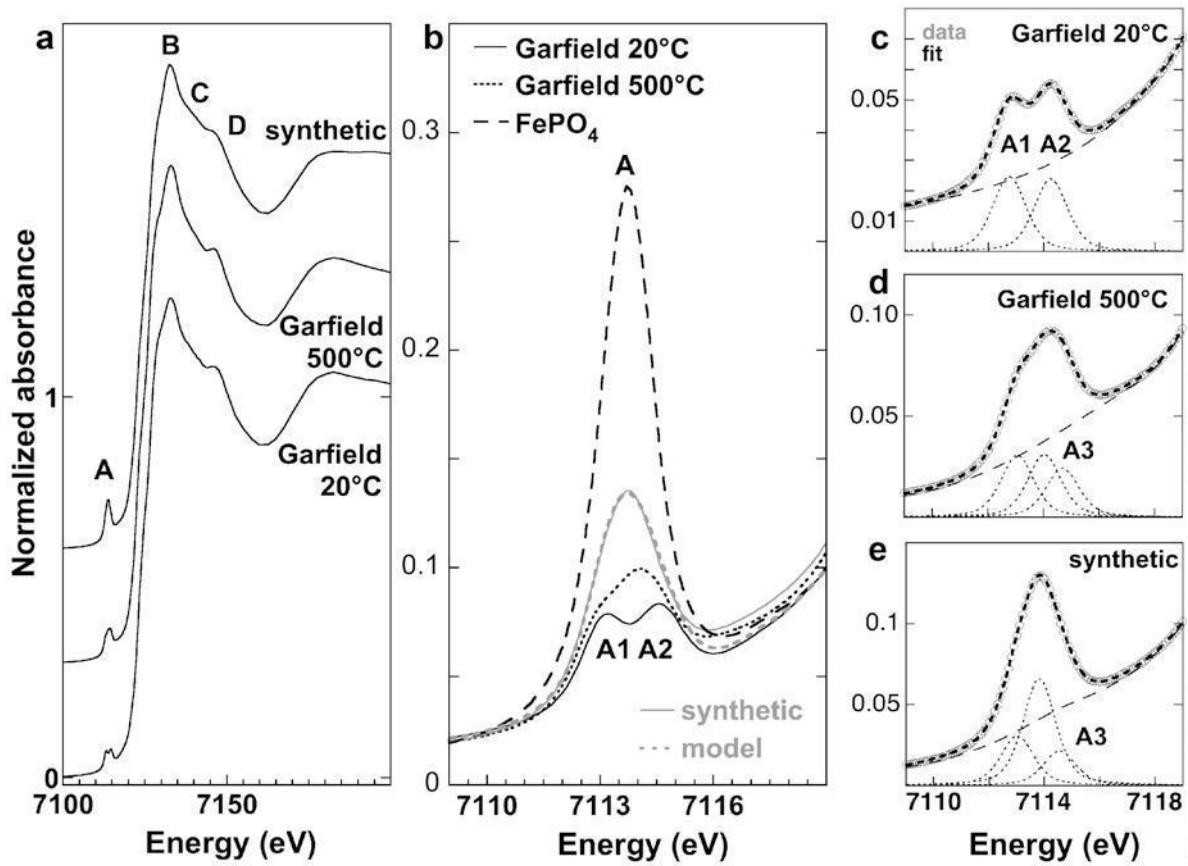

Figure 9. Normalized, high-resolution Fe K-edge XANES spectra of: (a) the synthesized nontronite (150ºC) and reference Garfield nontronite, as well as an inset on the pre-edge features (feature A); (b) normalized pre-edge feature for $FePO_4$ (dashed black line; Fe(III) is T_d), Garfield nontronite (solid black line; Fe(III) is O_h, centrosymmetric), heated (500ºC) nontronite (dotted black line; Fe(III) is O_h, but distorted; not C_{3v}) and the synthetic nontronite (solid gray line); also shown, the model (dotted gray line) of the pre-edge for the synthetic nontronite, using a mixing of $FePO_4$ and the Garfield nontronite spectra (25ºC). The pre-edge for the synthetic nontronite was also modeled using background-corrected pre-edge features as shown in (Figure 8c–e). The second transition for the synthetic nontronite is indicative of the presence of T_d, not distorted O_h or C_{3v}. Both methods yield similar amounts of T_d *vs.* O_h geometries around Fe(III).

that the Fe is present exclusively as Fe^{3+}, ~30% being located in the tetrahedral sites. So, according to all these consistent data and chemical analyses (Table 2), the synthesized clays are high-charge ferric nontronites, with the following structural formula:

$$(Si_{3.25}Fe^{3+}_{0.75})Fe^{3+}_2O_{10}(OH)_2.Na_{0.75}.$$

Nontronites with such chemistry are not known in nature. The Spokane, Washington, and Clausthal Zellerfeld, Germany, examples are the most Fe-rich nontronites described in the literature (Gates *et al.*, 2002). They contain some tetrahedral Al and some octahedral Mg. The synthesized nontronites are actually a theoretical, strictly ferric end-member on the beidellite/ferric-nontronite join. This smectite end-member formed at relatively low temperatures (75–150ºC), and could probably form at Earth-surface conditions. It is therefore possible to use this end-member in thermodynamic models of complex clay solid-solutions (Tardy and Fritz, 1981).

Within the temperature range 75–150ºC, a series of nontronites was synthesized, with the same layer charge (C_{12}-alkylammonium saturation data). The decrease in the synthesis temperature induces a lesser degree of crystallinity of nontronite: smaller diffracting domains in the layer plane, and fewer layers stacked coherently in tactoids (XRD data), even though the nontronite particles appear similar when examined using TEM. The temperature of formation of nontronite is, therefore, not the key parameter controlling the rate of Fe-for-Si tetrahedral substitution. The high level of tetrahedral Fe is probably linked to the increase in the thermodynamic stability of ferric-nontronites when the tetrahedral layer charge increases (Decarreau *et al.*, 2004).

Thermodynamic stability

Using a similar synthesis procedure described above, but working at 200ºC, aegirine was synthesized, mixed with small amounts of a ferric nontronite having a small

tetrahedral charge (Si−O FTIR band at 1010 cm^{-1}), and the chemical stability fields of aegirine, ferripyrophyllite, and nontronites were calculated (Decarreau *et al.*, 2004). Using the same chemical approach (Fe treated as an inert component in the sense of Thompson (1955)) and thermodynamics of aegirine, the stability fields of aegirine, ferripyrophyllite, and nontronites with various tetrahedral charges x (x = 0.33, 0.75) were calculated at several temperatures (Figure 10). The thermodynamic data for ferripyrophyllite and nontronites were calculated using algorithms from Vieillard (2000, 2002), improved using calorimetric measurements for phyllosilicates by Gailhanou (2005). Points 1, 2, and 3 on Figure 10 correspond to chemical data from Table 1. Points 9, 10, and 11 are chemical compositions of solutions in equilibrium with aegirine and low-charge nontronites (Decarreau *et al*., 2004). For the syntheses performed at temperatures between 75 and 150ºC (Figure 10a,b,c), the chemical compositions of solutions are in the stability field of high-charge (x = 0.75) nontronites, but near the aegirine−nontronite equilibrium. At 200ºC (Figure 10d), data points fall on the equilibrium line aegirine−low-charge nontronite (x = 0.33), consistent with Si−O FTIR data. The stability field of aegirine increases with temperature, while the stability field of nontronite is enlarged when the tetrahedral charge increases. Therefore, in the Si, Fe, Na, H_2O system, the largest $[Na^+]/[H^+]$ values favor the formation of aegirine, notably at high temperature (200ºC). At lower temperatures (75−150ºC), and medium values for $[Na^+]/[H^+]$, nontronites, especially with high charge, can form. This is probably the main reason (among others?) why high-charge nontronites were synthesized. On the contrary, when aegerine forms it is mixed with low-charge nontronites (Figure 10d). In any case, solutions were near the stability field of ferripyrophyllite. To form ferripyrophyllite, solutions must have high silica concentrations, low Na^+ concentrations, and acidic pH. In the present synthesis conditions, ferripyrophyllite generally does not form and a mixture of hematite and opal are obtained (Lantenois *et al.*, 2007).

Specific properties of the synthesized nontronite

Octahedral site occupancy. Fe-rich reference nontronites have a *tv* octahedral site occupancy (Besson *et al.*, 1983;

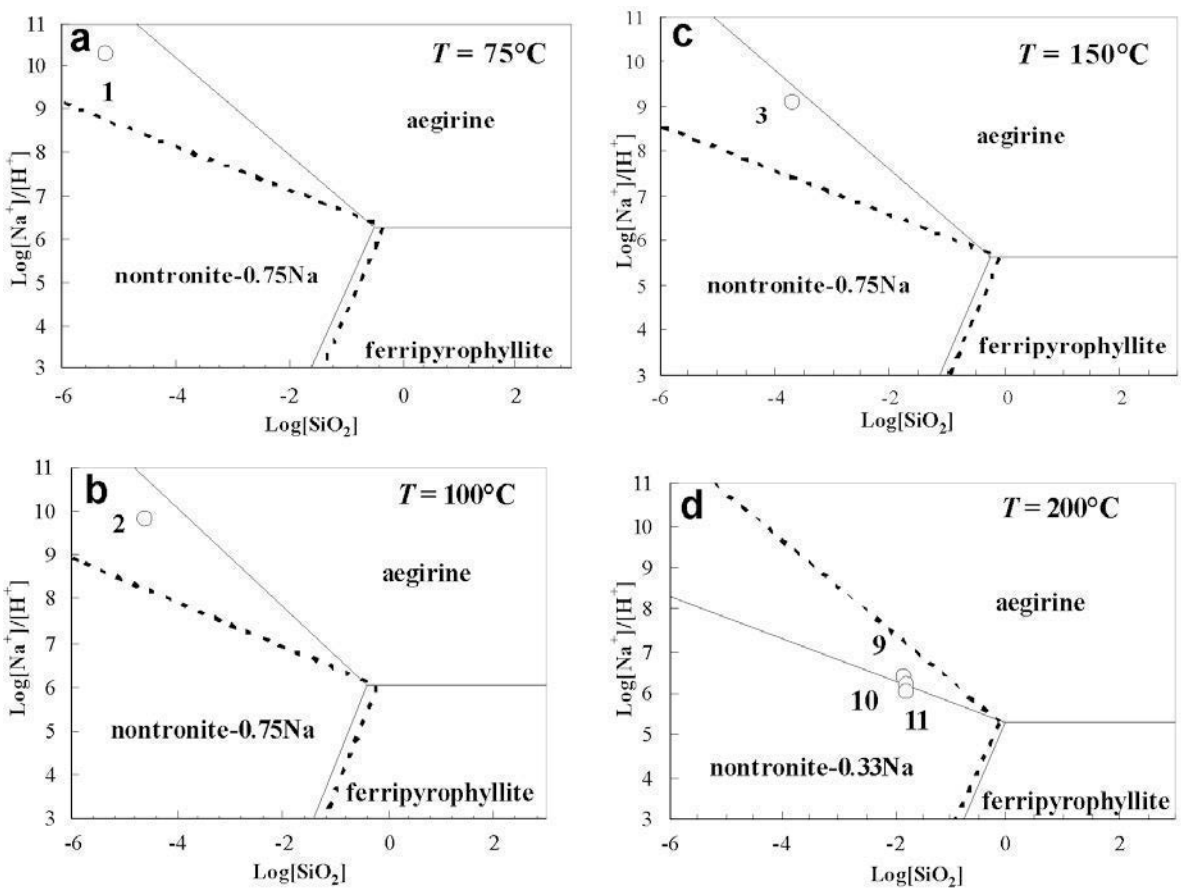

Figure 10. Thermodynamic stability diagrams of aegirine, ferripyrophyllite, and nontronites having the following structural formula: $(Si_{4-x}Fe^{3+}_x)Fe^{3+}_2O_{10}OH_2Na_x$. For a, b, and c, the continuous lines are for x = 0.75 and the dotted lines represent x = 0.33. It is the reverse for part d. For the chemical compositions of points 1, 2, 3, 9, 10, and 11, see text.

Tsipursky and Drits, 1984; Manceau *et al.*, 2000). Both Mössbauer and DTA-TG data of the synthesized nontronite are consistent with a *tv* structure. It appears that all dioctahedral 2:1 clays with a high Fe^{3+} octahedral content, either natural (celadonite, glauconite; (Daynyak *et al.*, 1981); ferripyrophyllite (Chukhrov *et al.*, 1979; Badaut *et al.*, 1992); nontronites (see above)) or synthesized, exhibit a *tv* structure. Such a generalized crystal chemistry feature of Fe-rich TOT clays probably has a thermodynamic origin.

Lattice parameters. The *b* parameter ($6 \times d_{06,33}$) of the synthesized nontronites is 9.24 Å. This value is high compared with those published for ferripyrophyllite (9.10 Å, Chukhrov *et al.*, 1979; Coey *et al.*, 1984; 9.06 Å, Badaut *et al.*, 1992) and Fe reference nontronites (9.06 Å for a SWa-1 sample, 9.13 Å for NG-1 and Garfield samples, Manceau *et al.*, 2000). As underlined previously (Eggleton, 1977; Brigatti, 1983; Manceau *et al.*, 2000), both octahedral Fe^{3+}-for-Al and tetrahedral Fe^{3+}-for-Si substitutions increase the *b* parameter values. The present data clearly show the strong increase of the *b* parameter when tetrahedral Fe^{3+} occurs. The tetrahedral Fe^{3+}-for-Si substitutions appear to be at least as efficient as the octahedral one. The *b* parameter value can then be simply used to evaluate the level of tetrahedral Fe, notably in synthesized nontronites: *e.g.* Mizutani *et al.* (1991) synthesized high-Fe, tetrahedrally substituted nontronites (*b* = 9.25 Å).

The value of the in-plane rotating angle, α, of adjacent tetrahedra can be calculated, using the classical approach of Bailey (1980) and an Fe^{3+}–O distance of 1.85 Å (Manceau *et al.*, 2000). For the synthesized nontronites, the calculated α angle is 10.47º, slightly above the value given for the Garfield nontronite (α = 7.7º, Manceau *et al.* 1998).

Dehydroxylation temperatures. For the synthetic nontronite obtained at 150ºC having the best crystallinity (similar to that of natural nontronites), the dehydroxylation temperature is 393ºC. It is the lowest dehydroxylation temperature measured for smectites, clearly linked to the high Fe content of this nontronite. Compared to the Garfield nontronite (458ºC), the dehydroxylation of the synthetic nontronite occurs at 65ºC less. This emphasizes the effect of tetrahedral Fe on the dehydroxylation temperature.

The decrease in the dehydroxylation temperature from 393 to 373ºC, when the synthesis temperature decreases from 150 to 75ºC, is explained by the concomitant decrease in crystallinity of the synthesized smectites as shown by the XRD and IR data. The DTA data reinforce the notion that dehydroxylation temperatures of clay minerals cannot be explained by their chemistry alone, but also by their crystallinity.

Identification of tetrahedral Fe and its distribution. Identification and quantification of tetrahedral Fe in smectites is generally not easy, in spite of the numerous methods that can be used (Mössbauer, XAFS, FTIR, XRD, *etc.* (Gates *et al.*, 2002)). Tetrahedral Fe was proven here by XRD, XAFS, FTIR, and Mössbauer spectroscopy. The XAFS appears as the most efficient method to prove and quantify the tetrahedral Fe. The quantification method used (Manceau *et al.*, 2000; Gates *et al.*, 2002) gives consistent results with C_{12}-alkylammonium saturation, Mössbauer, and chemical data. Despite the high level of tetrahedral Fe, the Mössbauer spectra do not exhibit any specific feature, and $^{IV}Fe^{3+}$ was proven only after decomposition, taking into account the high level of $^{IV}Fe^{3+}$ shown by other methods. Nevertheless, the amount of $^{IV}Fe^{3+}$ obtained by Mössbauer spectroscopy is consistent with all other data. The shift of the Si–O band in FTIR spectra toward lower frequency is also a clear feature of tetrahedral Fe but cannot be used easily to quantify it because total Fe and tetrahedral Al also influence this band position and calibrations must be made.

According to Mössbauer data, ~85% of octahedral Fe^{3+} ions are surrounded by a [3Si-Fe^{3+}] tetrahedral configuration (doublet 3), and 15% are surrounded by the [4Si] configuration (doublet 2). According to the structural formula, and on the basis of a random distribution of tetrahedral cations, the [4Si] configuration would be 44% and the [3Si-Fe^{3+}] configuration 40%. The high intensity of doublet 3 suggests that tetrahedral Fe atoms are not randomly distributed. The intensity ratio (*I*3/*I*2, Table 4) of these two doublets falls just below the curve corresponding to the cation distribution according to the Löwenstein rule by Besson *et al.* (1983) (*i.e.* the maximum octahedral Fe^{3+} surrounded by a [3Si-Fe^{3+}] tetrahedral configuration). For these synthesized smectites, the Loewenstein rule is thus obeyed. The intensity ratio *I*3/*I*2 is slightly too small, this is probably linked to uncertainties in Mössbauer fitting.

Gates *et al*. (2002) consider the Spokane County, Washington, nontronite as a smectite ferric end-member. Their data show that strictly ferric nontronites with greater tetrahedral charge can also be considered as end-members.

Expandability. After EG treatment, the synthesized nontronites show various behaviors, depending on their synthesis temperature and on their crystallinity. Despite the fact that all the nontronites are high-charge smectites, those exhibiting a high degree of crystallinity exhibit 'vermiculite-like' behavior, while those with a lower degree of crystallinity exhibit 'smectite-like' behavior (Suquet *et al.*, 1977). The present data show that expandability of TOT clays depends on their layer charge, but also on their crystallinity, *i.e.* the number of stacked layers, the mean crystal coherency in the layer plane, the particles size, *etc*.

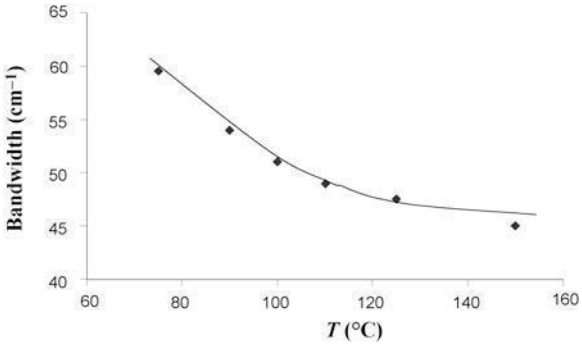

Figure 11. Width of the νFe_2^{3+}-OH FTIR band of nontronite as a function of synthesis temperature. The band width is correlated to the crystallinity of nontronites.

Smectites cannot exhibit larger crystals

When the synthesis temperature increases, the nontronite particles are thicker (Figure 5), and the XRD data clearly show an increase in crystallinity, notably a greater number of stacked layers and more extended crystal coherency in the layer plane (Figure 1). This evolution of crystallinity is also observed in FTIR spectra (Table 5). Increasing the synthesis temperature allows an improvement in the crystallinity of synthesized nontronites, as in many other clays (Carrado *et al.*, 2006). The measured bandwidth of the νFe_2^{3+}-OH *vs.* the synthesis temperatures are plotted in Figure 11. Improving the crystallinity of synthesized nontronites by changing synthesis conditions is clearly not possible. At a similar temperature (200ºC), using the same starting gel and duration of synthesis, euhedral crystals of aegirine, up to 2 µm long and 100 nm wide, were obtained (Decarreau *et al*., 2004). The small dimensions of the particles and the low crystallinity of synthesized (and natural) smectites cannot be explained by their chemistry or formation conditions, but, more likely, by their specific crystal growth of essentially bi-dimensional layers.

ACKNOWLEDGMENTS

We thank L. Daynyak for a fruitful preliminary discussion on Mössbauer data. We are grateful to C. Boissard (HydrASA laboratory, Université de Poitiers) for technical help (clay synthesis, XRD, FTIR). Associate Editor, P. Komadel, and the three reviewers are acknowledged for their constructive reviews.

REFERENCES

Badaut, D., Decarreau, A., and Besson, G. (1992) Ferripyrophyllite and related Fe $^{3+}$ rich 2:1 clays in recent deposits of Atlantis II deep, Read Sea. *Clay Minerals*, **27**, 227–244.

Bailey, S.W. (1980) Structures of layer silicates. Pp. 1–124 in: *Crystal Structures of Clay Minerals and their X-ray Identification* (G.W. Brindley and G. Brown, editors). Monograph **5**, Mineralogical Society, London.

Besson, G. and Drits, V. (1997) Refined relationships between chemical composition of dioctahedral fine-grained mica minerals and their infrared spectra within the OH stretching region. Part I: Identification of the stretching bands. *Clays and Clay Minerals*, **45**, 158–169.

Besson, G., Bookin, A.S., Dainyak, L.G., Rautureau, M., Tsipursky, S.I., Tcoubar, C., and Drits, V.A. (1983) Use of diffraction and Mössbauer methods for the structural and crystallochemical characterization of nontronites. *Journal of Applied Crystallography*, **16**, 374–383.

Bonnin, D. (1981) Propriétés magnétiques liées aux désordres bidimensionnels dans un silicate lamellaire ferrique: la nontronite. PhD thesis, Université Paris 6, France, 82 pp.

Brigatti, M. (1983) Relationships between composition and structure in Fe-rich smectites. *Clay Minerals*, **18**, 177–186.

Brindley, G.W. and Brown, G., editors (1980) *Crystal Structures of Clay Minerals and their X-ray Identification*. Monograph **5**, Mineralogical Society, London.

Calas, G. and Petiau, J. (1983) Coordination of iron in oxide glasses through high resolution K-edge spectra: information from the pre-edge. *Solid State Communications*, **48**, 625–629.

Carrado, K.A., Decarreau, A., Petit, S., Bergaya, F., and Lagaly, G. (2006) Synthetic clay minerals and purification of natural clays. Pp. 115–139 in: *Handbook of Clay Science* (F. Bergaya, B.K.G. Theng, and G. Lagaly, editors). Elsevier, Amsterdam.

Chukhrov, F.V., Zvyagin, B.B., Drits, V.A., Gorshov, A.I., Ermilova, L.P., Goilo, E.A., and Rudnistskaya, E.S. (1979) The ferric analogue of pyrophyllite and related phases. Pp. 55–64 in: *Proceedings of the International Clay Conference, Oxford, 1978* (M.M. Mortland and V.C. Farmer, editors). Elsevier, Amsterdam.

Coey, J.M.D. (1980) Clay minerals and their transformations studied with nuclear techniques: the contribution of Mössbauer spectroscopy. *Atomic Energy Review*, **18**, 73–124.

Coey, J.M.D. (1984) Mössbauer spectroscopy of silicate minerals. Pp. 443–509 in: *Mössbauer Spectroscopy Applied to Inorganic Chemistry* (G.J. Long, editor). Plenum Press, New York.

Coey, J.M.D., Chukhrov, F.V., and Zvyagin, B.B. (1984) Cation distribution, Mössbauer spectra and magnetic properties of ferripyrophyllite. *Clays and Clay Minerals*, **32**, 198–204.

Daynyak, L.G. and Drits, V.A. (1987) Interpretation of Mössbauer spectra of nontronite, celadonite and glauconite. *Clays and Clay Minerals*, **35**, 363–372.

Daynyak, L.G., Bookin, A.S., Drits, V.A., and Tsipursky, S.I. (1981) Mössbauer and electron diffraction study of cation distribution in celadonite. *Acta Crystallographica*, **A37**(suppl.), C-362.

Decarreau, A. and Bonnin, D. (1986) Synthesis and crystallogenesis at low temperature of Fe(III)-smectites by evolution of coprecipitated gels: experiments in partially reducing conditions. *Clay Minerals*, **21**, 861–877.

Decarreau, A., Bonnin, D., Badaut-Trauth, D., Couty, R., and Kaiser, P. (1987) Synthesis and crysytallogenesis of ferric smectite by evolution of Si-Fe coprecipitation in oxidizing conditions. *Clay Minerals*, **22**, 207–223.

Decarreau, A., Petit, S., Viellard, Ph., and Dabert, N. (2004) Hydrothermal synthesis of aegirine at 200ºC. *European Journal of Mineralogy*, **16**, 85–90.

Drits, V.A., Besson, G., and Muller, F. (1995) An improved model for structural transformations of heat-treated aluminous dioctahedral 2:1 layer silicates. *Clays and Clay Minerals*, **43**, 718–731.

Eggleton, R.A. (1977) Nontronite: chemistry and X-ray diffraction. *Clay Minerals*, **12**, 181–194.

Farges, F., Lefrère, Y., Rossano, S., Berthereau, A., Calas, G., and Brown, G.E., Jr. (2004) The effect of redox state on the

local environment of iron in silicate glasses: a combined XAFS spectroscopy, molecular dynamics, and bond valence study. *Journal of Non-Crystalline Solids*, **344**, 176–188.

Farmer, V.C., Krishnamurti, G.S.R., and Huang, P.M. (1991) Synthetic allophane and layer-silicate formation in SiO_2-Al_2O_3-FeO-Fe_2O_3-MgO-H_2O systems at 23ºC and 89ºC in calcareous environment. *Clays and Clay Minerals*, **39**, 561–570.

Fialips, C.-I., Huo, D., Yan, L., Wu, J., and Stucki, J.W. (2002) Effect of oxidation state on the IR spectra of Garfield nontronite. *American Mineralogist*, **87**, 630–641.

Gailhanou, H. (2005) Détermination expérimentale des propriétés thermodynamiques et étude des nanostructures de minéraux argileux. PhD thesis, Université Aix-Marseille III, Aix en Provence, France, 262 pp.

Gates, W.P. (2005) Infrared spectroscopy and the chemistry of dioctahedral smectites. Pp. 125–168 in: *The Application of Vibrational Spectroscopy to Clay Minerals and Layered Double Hydroxides* (J.T. Kloprogge, editor). CMS Workshop Lectures, Vol. **13**, The Clay Minerals Society, Aurora, Colorado.

Gates, W.P., Slade, P.G., Manceau, A., and Lanson, B. (2002) Site occupancies by iron in nontronites. *Clays and Clay Minerals*, **50**, 223–239.

Gillot, F., Righi, D., and Räisänen, M.L. (2001) Layer-charge evaluation of expandable clays from a chronosequence of podzols in Finland using an alkylammmonium method. *Clay Minerals*, **36**, 571–584.

Goodman, B.A. (1976) The effect of lattice substitutions on the derivation of quantitative site populations from Mössbauer spectra of 2:1 layer lattice silicates. *Journal de Physique Colloque*, **C6 37**, 819–823.

Goodman, B.A. (1978) The Mössbauer spectra of nontronite: consideration of an alternative assignment. *Clays and Clay Minerals*, **26**, 177–178.

Goodman, B.A., Russel, J.D., and Fraser, A.R. (1976) A Mössbauer and I.R. spectroscopy study of the structure of nontronite. *Clays and Clay Minerals*, **24**, 53–59.

Harder, H. (1976) Nontronite synthesis at low temperature *Chemical Geology*, **18**, 169–180.

Heller-Kallai, L. and Rozenson, I. (1981) The use of Mössbauer spectroscopy of iron in clay mineralogy. *Physics and Chemistry of Minerals*, **7**, 223–238.

Iriarte, I., Petit, S., Huertas, F.J., Fiore, S., Grauby, O., Decarreau, A., and Linares, J. (2005) Synthesis of kaolinite with a high level of Fe^{3+} for Al substitution. *Clays and Clay Minerals*, **53**, 1–10.

Keeling, J.L., Raven, M.D., and Gates, W.P. (2000) Geology and preliminary characterisation of two hydrothermal nontronites from weathered metamorphic rocks at the Uley graphite mine, South Australia. *Clays and Clay Minerals*, **48**, 537–548.

Kloprogge, J.T., Komarneni, S., and Amonette, J.E. (1999) Synthesis of smectite clay minerals: a critical review. *Clays and Clay Minerals*, **47**, 529–544.

Lagaly, G. (1994) Layer charge determination by alkylammonium ions. Pp. 1–46 in: *Layer Charge Characteristics of 2:1 Silicate Clay Minerals* (A.R. Mermut, editor). CMS Workshop Lectures, vol. **6**. The Clay Minerals Society, Boulder, Colorado, USA.

Lantenois, S., Beny, J.M., Muller, F., and Campallier, R. (2007) Integration of Fe in natural and synthetic Al-pyrophyllites: an infrared spectroscopy study. *Clay Minerals*, **42**,129–141.

Luca, V. (1991) Detection of tetrahedral Fe^{3+} sites in nontronite and vermiculite by Mössbauer spectroscopy. *Clays and Clay Minerals*, **39**, 467–477.

Madejová, J., Komadel, P., and Čičel, B. (1994) Infrared study of octahedral site populations in smectites. *Clay Minerals*, **29**, 319–326.

Mackenzie, R.C. (1970) *Differential Thermal Analysis* (R.C. Mackenzie, editor). Academic Press, London.

Manceau, A., Chateigner, D., and Gates, W.P. (1998) Polarized EXAFS, distance-valance least-squares modeling (DLVS), and quantitative texture analysis approaches to the structural refinement of Garfield nontronite. *Physics and Chemistry of Minerals*, **25**, 347–365.

Manceau, A., Lanson, B., Drits, V.A., Chateigner, D., Gates, W.P., Wu, J., Huo, D., and Stucki, J.W. (2000) Oxidation-reduction mechanism of iron in dioctahedral smectites: I. Crystal chemistry of oxidized reference nontronites. *American. Mineralogist*, **85**, 133–152.

Mineeva, R.M. (1978) Relationship between Mössbauer spectra and defect structure in biotites from electric gradient calculations. *Clays and Clay Minerals*, **2**, 267–277.

Mizutani, T., Fukushima, Y., Okada, A., Kamigaito, O., and Kobayahi, T. (1991) Synthesis of 1:1 and 2:1 iron phyllosilicates and characterization of their iron state by Mössbauer spectroscopy. *Clays and Clay Minerals*, **39**, 381–386.

Muller, F., Drits, V.A., Plançon, A., and Robert, J.L. (2000) Structural transformation of 2:1 dioctahedral layer silicates during dehydroxylation-rehydroxylation reactions. *Clays and Clay Minerals*, **48**, 572–585.

Nagase, T., Iwasaki, T., Ebina, T., Hayashi, H., Onodera, Y., and Dutta, N.C. (1999) Hydrothermal synthesis of Fe-montmorillonite in Si-Fe-Mg system. *Chemistry Letters*, 303–304.

Olis, A.C., Malla, P.B., and Douglas, L.A. (1990) The rapid estimation of the layer charge of 2:1 expanding clays from a single alkylammonium ion expansion. *Clay Minerals*, **25**, 39–50.

Rancourt, D.G., McDonald, A.M., Lalonde, A.E., and Ping, J.Y. (1993) Mössbauer absorber thickness for accurate site populations in Fe-bearing minerals. *American Mineralogist*, **78**, 1–7.

Reynolds, R.C. (1985) *NEWMOD: A Computer Program for the Calculation of One- dimensional Diffraction Powders of Mixed-Layer Clays*. Published by the author, R.C. Reynolds, 8 Brook Rd., Hanover, New Hampshire 03755 USA, 315 pp.

Slominskaya, M.V., Besson, G., Dainyak, L.G., Tchoubar, C. and Drits, V.A. (1986) Interpretation of the IR spectra of celadonites and glauconites in the region of the OH-stretching frequencies. *Clay Minerals*, **21**, 377–388.

Suquet, H., Iiyama, J.T., Kodama, H., and Pezerat, H. (1977 Synthesis and swelling properties of saponites with increasing layer charge. *Clays and Clay Minerals*, **25**, 231–242.

Tardy, Y. and Fritz, B. (1981) An ideal solution model for calculating solubility of clay minerals. *Clay Minerals*, **16**, 361–373.

Thompson, J. B. (1955) The thermodynamic basis for the mineral facies concept. *American Journal of Science*, **53**, 65–103.

Tsipursky, S.I. and Drits, V.A. (1984) The distribution of octahedral cations in 2:1 layers of dioctahedral smectites studied by oblique texture electron diffraction. *Clay Minerals*, **19**, 177–192.

Vieillard, P. (2000) A new method for the prediction of Gibbs free energies of formation of hydrated clay minerals based on the electronegativity scale. *Clays and Clay Minerals*, **48**, 459–473.

Vieillard, P. (2002) A new method for the prediction of Gibbs free energies of formation of phyllosilicates (10 Å and 14 Å) based on the electronegativity scale. *Clays and Clay Minerals* **50**, 352–363.

Westre, T.E., Kennepohl, P., de Witt, J., Hedman, B., Hodgson, K.O., and Solomon, E.I. (1997) A multiplet analysis of Fe K-edge 1s → 3d pre-edge features of iron

complexes. *Journal of the American Chemical Society*, **119**, 6297–6314.

Wilke, M., Farges, F., Petit, P.-E., Brown, G.E. Jr., and Martin, F. (2001) Oxidation state and coordination of Fe in minerals: an Fe K-XANES study. *American Mineralogist*, **86**, 714–730.

Zviagina, B., McCarty, D.K., Środoń, J., and Drits, V.A. (2004) Interpretation of infrared spectra of dioctahedral smectites in the region of OH-stretching vibrations. *Clays and Clay Minerals*, **52**, 399–410.

(*Received 25 September 2007; revised 28 January 2008; Ms. 0077; A.E. P. Komadel*)